J Comput Electron (2012) 11:67–77
DOI 10.1007/s10825-012-0392-0

Thermoelectric performance of disordered and nanostructured graphene ribbons using Green's function method

Fulvio Mazzamuto · Jérôme Saint-Martin · Viet Hung Nguyen · Christophe Chassat · Philippe Dollfus

Published online: 16 February 2012

Abstract The thermoelectric properties of defected graphene nanoribbons (GNRs) and multi-junction (MJ) GNRs coupling periodic armchair sections of different width are analyzed by means of Green's function techniques to simulate electron and phonon transport. Among the different strategies likely to enhance the thermoelectric performance, the effects of edge disorder and random vacancies are shown to be small since they lead to the concomitant degradation of the phonon thermal conductance and of the electronic conductance, which finally reduces the thermoelectric factor ZT. However, the periodic distribution of vacancies and the structuring of GNRs in MJ-GNRs both lead to the enhancement of the figure of merit ZT. In the latter case, in addition to the strong reduction of the phonon thermal conductance, an effect of resonant tunneling of electrons allows retaining high electronic conductance and enhancing significantly the thermopower. Finally, by introducing a periodic distribution of vacancies in the MJ-GNR, the maximum value $ZT = 0.4$ is reached at room temperature.

Keywords Graphene · Phonon transport · Thermal effects · Thermoelectrics · Green's function

F. Mazzamuto · J. Saint-Martin · V.H. Nguyen · C. Chassat · P. Dollfus (✉)
Institute of Fundamental Electronics (IEF), CNRS, UMR 8622, Univ. Paris-Sud, Orsay, France
e-mail: philippe.dollfus@u-psud.fr

V.H. Nguyen
Institute of Physics, Vietnamese Academy of Science and Technology, Hanoi, Vietnam

1 Introduction

Beyond its exceptional electron transport properties and potential for high speed electronics [1, 2], graphene has recently attracted attention for its thermal [3–5] and thermoelectric [6, 7] properties. The performance of thermoelectric materials is measured through a unitless parameter, ZT, which is called thermoelectric figure of merit and is defined as $G_e S^2 T/K$, where G_e is the electrical conductance, S is the Seebeck coefficient (or thermoelectric power), $K = K_e + K_{ph}$ is the thermal conductance including both electron and phonon contributions, and T is the temperature. Due to the strong interdependence of these quantities it is difficult to envision a strategy of material engineering likely to provide a room-temperature ZT higher than 1, i.e. higher than that already obtained in the 1950s with Bi_2Te_3 alloys [8]. In the 1990s the pioneering work of Hicks and Dresselhauss [9, 10] has introduced the idea that quantum confinement of carriers and nanostructuring of materials may increase ZT beyond the critical value of 1. Intense research in this direction has led to successful results with superlattices [11, 12], quantum dots [13–15] and nanowires [16, 17]. However, these nanostructures have taken advantage mainly of reduced phonon thermal conductance while the confinement of carriers did not have a significant effect. It is particularly true in the case of Si nanowires where the Seebeck coefficient and the electrical conductance are the same as in bulk-Si while the thermal conductivity is reduced by two orders of magnitude, probably because of surface roughness effects [16].

Due to its thermal conductivity as high as 5 kW m^{-1} K^{-1} [4], graphene was not initially expected to be a good candidate for thermoelectrics. However, recent works based on numerical simulation have suggested that high ZT values could be reached in simple honeycomb chains of carbon atoms [18], in long rough-edge graphene nanoribbons

(GNRs) [19], in GNRs with atomic vacancies [20], or in graphene anti-dot lattices [21]. Recently, we have demonstrated that the nanostructuring of GNRs by alternating armchair and zigzag GNR sections of different width makes it possible to benefit from both a reduced phonon thermal conductance and a resonant tunneling effect for electrons which preserves the electronic conductance and enhances the Seebeck coefficient compared to perfect armchair GNR. This configuration has led to ZT values of about 1 at room temperature [22].

In this article, we examine different mechanisms and concepts of structuring which may have an influence on the thermoelectric performance of GNRs: edge disorder, random vacancy distribution, periodic distribution of vacancies and nanostructuring of GNRs in periodic armchair sections of different width. The electron and phonon transport equations are treated on an equal footing using the non-equilibrium Green's function approach for the computation of the electron and phonon transmissions on the basis of an atomistic real-space description of GNRs.

Actually, different semi-classical and quantum approaches have been developed to describe the phonon transport in nanostructures such as the Monte Carlo solution of the Boltzmann equation [23], the molecular dynamics [24, 25], the transfer matrix [26], the order-N real-space Kubo formalism [27], or the NEGF method [28]. The NEGF method is also widely used to simulate the quantum transport of charges in graphene devices by considering either the continuous Dirac Hamiltonian in large graphene samples [29–31] or an atomistic tight-binding Hamiltonian in GNRs [32–38]. It has been used also to compute simultaneously electron and phonon transport in graphene structures, which gives access to their thermoelectric properties [19–22, 39]. In most of these works, a simple nearest-neighbor tight-binding (NNTB) Hamiltonian without edge relaxation was used for electrons, while a force constant model (FCM) including the fourth nearest-neighbors or less was considered for phonons [19, 39]. It should be noted that a third NNTB model was used for electrons in [21]. In the present work, a lattice dynamic equation based on a fifth nearest-neighbor FCM [40, 41] and a first NNTB electron Hamiltonian including armchair edge relaxation [22, 36] have been used.

This article is organized as follows. In Sect. 2, the models used to compute the states and transport of electrons and phonons are described. In Sect. 3, the results obtained are presented and discussed. We summarize and draw some conclusions in Sect. 4.

2 Model

In semiconducting nanostructures such as silicon nanowires, it is important to include all sources of scattering in the simulation, in particular electron-phonon scattering, to extract accurate thermoelectric parameters [42]. However, in 2D graphene the mean free path of electrons and phonons at room temperature is typically higher than 400 nm [43] and 775 nm [4], respectively, i.e. much longer than the structures simulated here. In GNRs the electron mobility is essentially limited by vacancies and edge disorder [44] and the electron-phonon coupling is weak [45]. Accordingly, in our model both phonon and electron populations are assumed to travel ballistically and independently, as commonly assumed in thermoelectric studies of GNRs [19–21]. The anharmonicity of the atomic interactions is thus neglected in the calculation of phonon transport properties. Basically, the electron (phonon) transmission function T_e (T_{ph}) is deduced from the Green's functions of the electron Schrödinger equation (lattice dynamic equation). The Landauer formalism is then applied to calculate the phonon and electron fluxes and all related quantities.

2.1 Electronic band structure and electron transport

To model the electron behavior in GNR devices connected to two leads, we consider the Hamiltonian of the general form

$$H = H_D + H_L + H_R + H_{DL} + H_{DR}, \tag{1}$$

where H_D is the Hamiltonian of the device, $H_{L,R}$ are the Hamiltonians of the left and right leads, respectively, and H_{DL} and H_{DR} describe the coupling of the device to the leads. These Hamiltonians can be expanded in terms of creation and annihilation operators at each atomic site, and to describe the electronic structure of graphene, a single band tight-binding model can be used, with $a_c = 0.142$ nm as carbon-carbon distance and $t = 2.7$ eV as overlap integral between p_z orbitals [43, 46]. However, first-principles simulations have shown that the relaxation of armchair edges significantly changes the edge bond length and tight-binding parameters [47], while this effect has been predicted to be much smaller for zigzag edge bonds [48]. In the present work the bond relaxation is included using two different TB parameters: the hopping energy $t_{edge} = 3.02$ eV is used for armchair-edge bonds [47] and the standard value $t = 2.7$ eV [46] is used for internal and zigzag-edge bonds. It is worth noting that for AGNRs which are found to be metallic when using a single hopping parameter, a small band gap opens when considering the edge relaxation through a specific edge hopping parameter. In the following, such AGNRs will be referred to as "quasi-metallic".

In the Green's functions (GFs) language [49], the device retarded Green's function is defined as

$$G_D^r(E) = \left[E + i\eta - H_D - \Sigma_L^r - \Sigma_R^r\right]^{-1}, \tag{2}$$

where the retarded self-energies Σ_R^r and Σ_L^r describe the device-lead couplings and contain the information on the

electronic structure of the semi-infinite leads. For instance, the self-energy of the left lead can be expressed as

$$\Sigma_L^r(E) = H_{DL} g_L^r(E) H_{LD}, \tag{3}$$

where $g_L^r(E)$ is the surface GF of the uncoupled left lead, with similar definitions for the self-energy of the right lead. The surface GFs and the device GFs are calculated using the fast iterative scheme described in [50] and the recursive algorithm proposed in [51], respectively. The local density of states (LDOS) at site j can be extracted from the retarded GF as

$$LDOS_{(j)} = -2 \operatorname{Im} G^r(j,j). \tag{4}$$

By introducing the advanced GF $G_D^a(E) = G_D^r(E)^\dagger$ and self-energies $\Sigma_{L,R}^a(E) = \Sigma_{L,R}^r(E)^\dagger$, one can compute the particle injection rates at contacts

$$\Gamma_{L,R}(E) = i\big[\Sigma_{L,R}^r(E) - \Sigma_{L,R}^a(E)\big] = -2 \operatorname{Im}\big[\Sigma_{L,R}^r(E)\big], \tag{5}$$

and the transmission function

$$T_e(E) = \operatorname{Tr}\big[\Gamma_L(E) G_D^r(E) \Gamma_R(E) G_D^a(E)\big]. \tag{6}$$

The electronic conductance G_e is then deduced as a function of the Fermi energy μ as

$$G_e(\mu) = \frac{2e}{h} T_e(\mu). \tag{7}$$

The thermopower S and the electronic contribution to the thermal conductance K_e can be derived via the intermediate L_n functions defined as [20, 52]

$$L_n(\mu, T) = \frac{2}{h} \int T_e(E)(E-\mu)^n \frac{-\partial f(E,\mu,T)}{\partial E} dE, \tag{8}$$

where $f(E,\mu,T)$ is the Fermi-Dirac distribution function at temperature T. Finally, S and K_e are expressed and computed as

$$S(\mu, T) = \frac{1}{eT} \frac{L_1(\mu,T)}{L_0(\mu,T)}, \tag{9}$$

and

$$K_e(\mu, T) = \frac{1}{T}\left[L_2(\mu,T) - \frac{L_1(\mu,T)^2}{L_0(\mu,T)}\right]. \tag{10}$$

2.2 Phononic structure and phonon thermal conductance

In the small displacement limit, the equation of motion of the i-th atom writes

$$m \frac{d^2 \vec{u}_i}{dt^2} = \sum_j k_{ij}(\vec{u}_j - \vec{u}_i), \tag{11}$$

where $\vec{u}_j$ is the relative displacement vector of the j-th atom, k_{ij} is the force constant parameter describing the coupling between the i-th and the j-th atom, and m is the mass of carbon atoms. A fifth nearest-neighbor force constant model is used to describe the interaction between atoms, with coupling parameters determined in [40]. For a finite structure of N atoms, the system of equations (11) may be written in a matrix form, which, after Fourier transform, can be expressed as a function of the angular frequency of atomic vibrations ω as

$$\big[\omega^2 M - K\big] U = 0, \tag{12}$$

where U is the column vector formed by all relative displacement vectors $\vec{u}_j$, M is the mass tensor of carbon atoms and K is the dynamic matrix. The eigenvalues ω^2 of (12) correspond to the vibration frequencies of the lattice, i.e. to the phonon modes. Here, K plays the same role as the Hamiltonian H for electrons. Similarly to the Hamiltonian in (1), it can be decomposed in different sub-parts as

$$K = K_D + K_L + K_R + K_{DL} + K_{DR}. \tag{13}$$

As for the electron GF defined in (2) the device retarded Green's function of the dynamic equation (12) is defined as

$$G_D^r(\omega) = \big[\omega^2 M + i\eta - K_D - \Sigma_L^r - \Sigma_R^r\big]^{-1}, \tag{14}$$

where the self-energies Σ_L^r and Σ_L^r describing the lead-to-device coupling are defined as in (3). With phonon injection rates defined as in (5) the phonon transmission function finally writes

$$T_{ph}(\omega) = \operatorname{Tr}\big[\Gamma_L(\omega) G_D^r(\omega) \Gamma_R(\omega) G_D^a(\omega)\big]. \tag{15}$$

In the case of ballistic phonons, the lattice contribution to the thermal conductance is given by [53]

$$K_{ph} = \int T_{ph}(\omega) \left[\frac{\partial n(\omega,T)}{\partial T}\right] \frac{\hbar\omega}{2\pi} d\omega, \tag{16}$$

where $n(\omega,T)$ is the Bose-Einstein distribution function. This general expression can be conveniently rewritten in the form [54]

$$K_{th}(T) = \frac{1}{8\pi k_B T^2} \int_0^\infty \hbar^2 \omega^2 \frac{T_{ph}(\omega)}{\sinh^2(\frac{\hbar\omega}{2k_B T})} d\omega. \tag{17}$$

Finally, by regrouping (7), (9), (10) and (17), the thermoelectric figure of merit is computed as

$$ZT = \frac{G_e S^2}{K_e + K_{ph}} T. \tag{18}$$

2.3 Simulated structures and preliminary results

The GNRs are defined by their edge orientations and by the number n of dimers in the unit cell which is related to the ribbon width W. In this article we focus on GNRs with armchair edges, denoted as n-AGNRs, the width of which is expressed as

$$W = \frac{1}{2}(n-1)a_c. \tag{19}$$

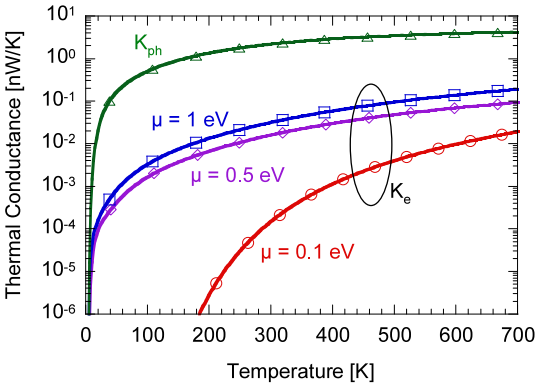

Fig. 1 Electron and phonon contributions K_e and K_{ph}, respectively, to the thermal conductance K for a 15-AGNR as a function of temperature T. K_e is plotted for three values of electron chemical potential

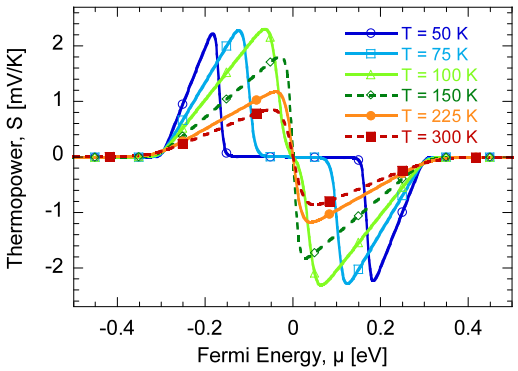

Fig. 2 Seebeck coefficient (or thermopower) of a 15-AGNR as a function of chemical potential μ for different temperatures

We will consider also a multi-junction AGNR (MJ-AGNR) obtained by alternating periodically AGNR slices of different width. All simulated structures consist in a GNR active zone coupled with two semi-infinite contacts with the same structure.

In the result Sect. 3, only the phonon contribution to the thermal conductance will be presented and discussed, the electron contribution being considered as smaller. This assumption is fully true in perfect GNRs, as shown in Fig. 1 where we compare the electron and phonon contributions to the thermal conductance as a function of temperature and for different values of electron chemical potential. The phonon contribution is always at least one order of magnitude higher than the electron contribution, even for high electron chemical potential. However, it should be noted that (i) this is no longer true in nanostructured GNRs where the phonon conductance is strongly reduced and may become similar to the electron thermal conductance and (ii) both contributions were included in the computation of ZT (18) in all results presented below.

The effect of temperature on the Seebeck coefficient S is more complex. In contrast to the case of 2D graphene where the S peaks are almost independent of temperature and electron chemical potential [20], in GNRs the maximum value of S is temperature-dependent at high temperature and the position of peaks is energy-dependent at low temperature, as shown in Fig. 2 for a 15-AGNR. Due to the symmetry between conduction and valence bands, S is always zero when the chemical potential is at the middle of the band gap, i.e. for $\mu = 0$. For positive energies, according to (9) the maximum S occurs when the value of $E - \mu$ weighted by the electron transmission T_e is maximized. The effect of bandgap on S is mainly visible at low temperature ($T < 100$ K here) through a plateau around $\mu = 0$.

The effects of GNR width and orientation on all parameters involved in the evaluation of ZT have been discussed in detail elsewhere [22]. In the next section we focus on AGNRs with $n = 16$ dimers in the unit cell and we discuss the effects of edge disorder, vacancies and structuring of ribbons in multi-junction structures.

3 Results and discussion

3.1 Edge disorder effects

The thermoelectric properties of AGNRs are first analyzed as a function of the edge disorder. To understand how the edge quality may affect the figure of merit ZT, we compare the results obtained for 16-AGNRs with different edge roughness parameters. We define a roughness index as the probability for each edge dimer to be removed. The disorder is limited to the edge dimers and the possibility of deeper roughness is not taken into account here. In Fig. 3 we compare a perfect 16-AGNR to three 16-AGNRs with roughness index of 5%, 10% and 15%, respectively, for a device length $L = 20$ nm. For all structures, schematized in Fig. 3(a), we plot the phonon thermal conductance as a function of temperature in Fig. 3(b), while the electronic conductance G_e, the Seebeck coefficient S and the figure of merit ZT are plotted at room temperature as a function of the chemical potential μ in Figs. 3(c), 3(d) and 3(e), respectively.

Figure 3(b) shows clearly that edge disorder tends to degrade significantly the phonon thermal conductance which decays from 2.4 nW K^{-1} for the perfect GNR to about 1.6 nW K^{-1} for the disordered GNRs at room temperature. The results shown for roughness indices of 5% and 10% seem similar but it is actually fortuitous. Indeed, these two results correspond to two specific distributions of defects selected randomly. If the thermal conductance is averaged over a large number of disordered GNRs, a continuous decrease is observed when increasing the roughness index in the range 0–15% (not shown here).

In principle, according to (18), this reduction of thermal conductance induced by edge disorder is likely to enhance the figure of merit ZT. However, it is not the case here because the edge disorder also affects the electronic transport

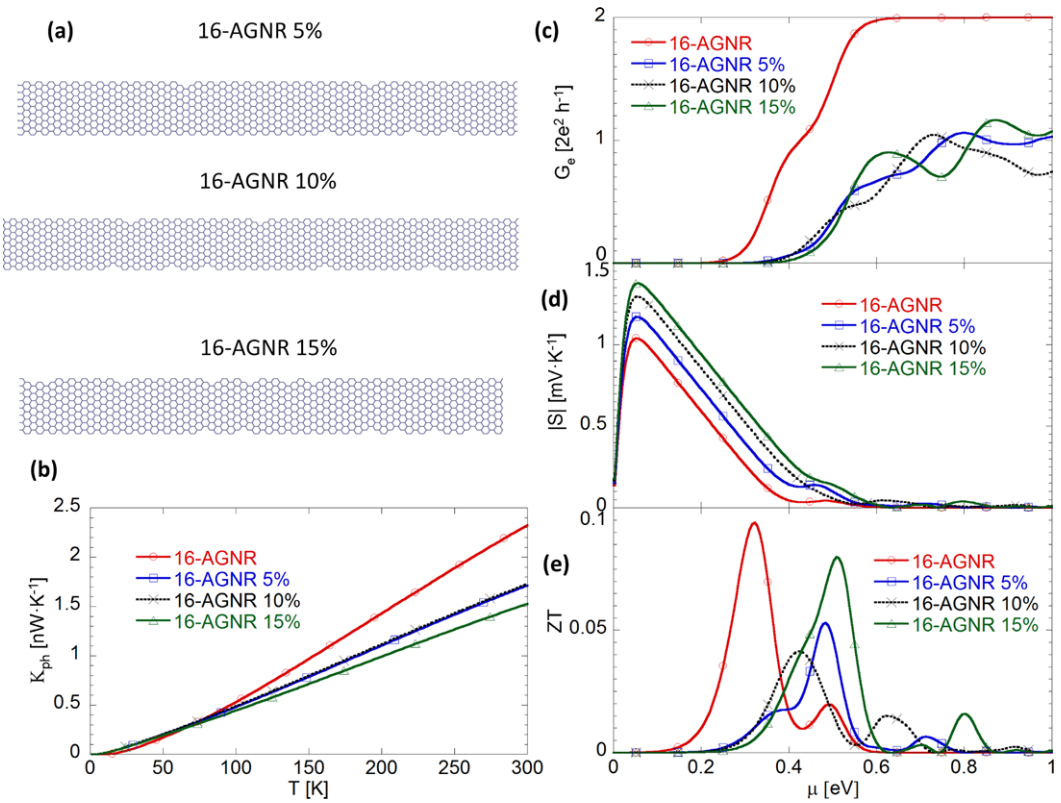

Fig. 3 (**a**) 16-AGNR structure with different values of roughness index: 5%, 10% and 15%. (**b**) Phonon thermal conductance as a function of temperature T, (**c**) electronic conductance, (**d**) Seebeck coefficient and (**d**) figure of merit ZT as a function of chemical potential μ for the perfect 16-AGNR and for 16-AGNRs with edge disorder as schematized in (**a**)

properties with negative overall consequences on ZT. More precisely, two main effects on the electronic transport can be identified:

– A positive effect: the enhancement of the electronic bandgap, which can be seen directly on the electronic conductance plotted in Fig. 3(c) or indirectly on the Seebeck coefficient displayed in Fig. 3(d). Indeed, a previous study of the effect of GNR width on the thermoelectric properties has shown a linear relationship between the bandgap and the maximum value of S [22], in agreement with theoretical predictions [55]. This overall tendency is confirmed here with the small enhancement of height and width of the Seebeck coefficient peak when increasing the roughness (Fig. 3(d)) while the bandgap of rough AGNRs is more than 100 meV higher than that of the perfect AGNR.
– A negative effect: the reduction of electronic conductance, as shown in Fig. 3(c) for all roughness indexes. Additionally, the random edge profiles induce random oscillations of electronic conductance at high energy.

The global electron transport properties for thermoelectricity may be analyzed through the single quantity G_eS^2, often referred to as the power factor. In rough AGNRs, the reduction of electronic conductance is strong enough to reduce also the power factor and even to loose fully the benefit of the reduced thermal conductance. Finally, the ZT peaks of rough GNRs are all smaller than that of the perfect AGNR (Fig. 3(e)). Additionally, the peak ZT values and their energy position strongly depend on the random edge profile which is impossible to control. Hence, the edge roughness cannot be considered as a viable way to improve the thermoelectric properties of short GNRs. It may be seen as a contradiction with the results reported for long GNRs in [19]. However, these results were obtained by introducing empirically a finite phonon mean free path which in long GNRs induces a strong localization of phonons and reduces drastically the thermal conductance. This assumption does not hold for the small structures considered here.

3.2 Effect of vacancies

The analysis is quite different if the atomic vacancies are located inside the ribbon lattice and not only at the edges. Two types of vacancy distributions are considered here: (i) atomic vacancies are spread randomly in the lattice, or (ii) atomic vacancies are distributed periodically to form a 1D chain in the center of the ribbon. To analyze the main

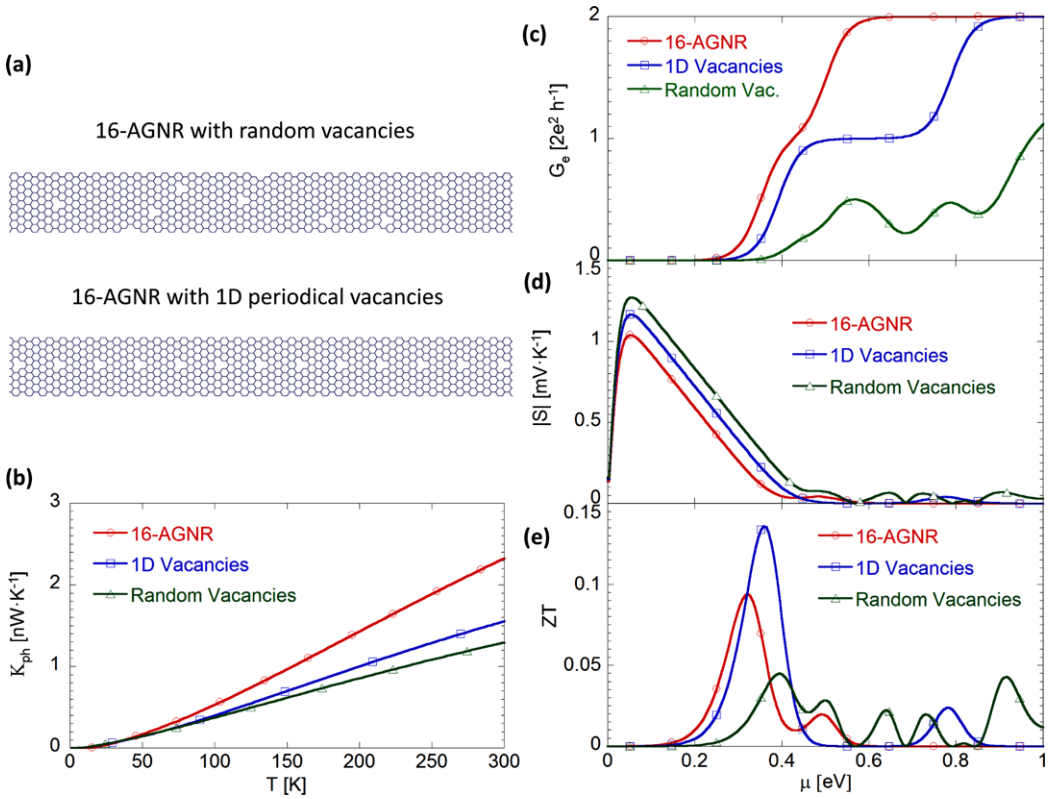

Fig. 4 (**a**) 16-AGNR structure with random vacancies and with periodic distribution of vacancies. (**b**) Thermal conductance as a function of temperature T, (**c**) electronic conductance, (**d**) Seebeck coefficient and (**e**) figure of merit ZT as a function of chemical potential μ

effects of such vacancies we compare a perfect 16-AGNR to two 16-AGNRs with vacancy distributions as schematized in Fig. 4(a). To make relevant comparisons the three structures have the same active region length, i.e. 30 armchair unit cells corresponding to $L = 13$ nm, and the two defective GNRs present the same density of atomic vacancies, i.e. about one vacancy per 100 lattice atoms. For the three structures, we plot the thermal conductance as a function of the temperature in Fig. 4(b), the electronic conductance, the Seebeck coefficient and the figure of merit ZT as a function of the chemical potential in Figs. 4(c), 4(d) and 4(e), respectively.

The general conclusion that the thermal conductance strongly decreases in defective GNRs is not only valid in the case of edge roughness but also for atomic vacancies inside the ribbon. This is confirmed in Fig. 4(b) where the phonon thermal conductance of the 16-AGNR with random vacancies is almost two times smaller than for the perfect 16-AGNR. The degradation is slightly less pronounced for the 16-AGNR with periodical distribution of vacancies.

As shown for rough GNRs, the thermal conductance reduction does not always lead to the enhancement of ZT because of the concomitant degradation of electronic transport. Regarding this point, introducing vacancies in the GNR yields the same two phenomena as observed in rough GNRs: the band gap is enhanced and the electronic conductance tends to be reduced. These effects appear clearly in Fig. 4(c). In particular, with respect to perfect GNR, the energy gap increases by about 50 meV with periodical vacancies and by more than 100 meV for random vacancies. Accordingly, the enhancement of the Seebeck coefficient is observed in Fig. 4(d). However, there is a significant difference between the two defective GNRs. For the GNR with random vacancies the electronic conductance is strongly degraded and exhibits random oscillations. In the case of periodical vacancies the oscillations are not detected and the electronic conductance has the classical step-like shape of perfect GNRs. This behavior can be interpreted as a reduction of the effective width of the ribbon. If vacancies are periodically distributed at the center of the ribbon, the electron conduction is separated over two coherent lateral sub-ribbons which behave like a single GNR of smaller width. It is known that the electronic and thermoelectric properties strongly depend on the GNR width [22]. In particular, as mentioned above one of the main effect of width reduction is the enhancement of band bap with a subsequent proportional enhancement of the Seebeck coefficient. More generally, in narrow GNRs the power factor $G_e S^2$ increases and the thermal conductance decreases to the benefit of the thermoelectric figure of merit. The same tendency is observed here for periodi-

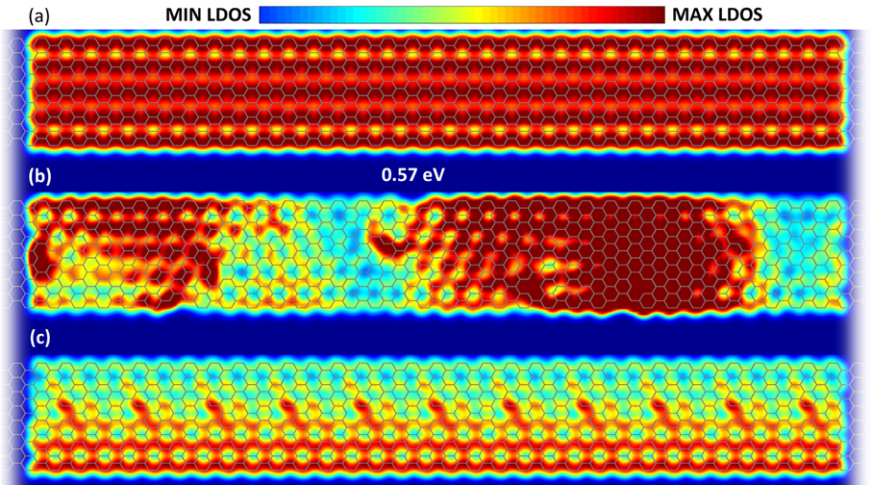

Fig. 5 Electronic LDOS calculated at 0.57 eV for (**a**) perfect 16-AGNR, (**b**) 16-AGNR with random vacancies and (**c**) 16-AGNR with periodical vacancies

cal vacancies. Figure 4(d) shows how the height of the main *ZT* peak decreases from 0.08 for the perfect 16-AGNR to 0.03 in the case of random vacancies because of the strong degradation of electronic transport, but increases to 0.13 in the case of periodical vacancies thanks to the effective width reduction.

The analysis of the electron local density of states (LDOS) is helpful to interpret the results obtained and to confirm our understanding of the effects of random and periodic vacancies. We plot in Fig. 5, the electron LDOS calculated for the three structures at the energy 0.57 eV which corresponds to the first maximum of electronic conductance for the 16-AGNR with random vacancies. As expected, the LDOS of the perfect AGNR, displayed in Fig. 5(a), is uniform over the length of the ribbon and the electronic states are distributed over the full width. This is not the case of the AGNR with random vacancies (Fig. 5(b)). In this structure the vacancies break the homogeneous distribution of states and generate their partial localization which is responsible for the strong reduction of electronic conductance. Finally, Fig. 5(c) confirms that the periodic 1D chain of vacancies separate the GNR in two non-symmetric sub-ribbons. At this particular energy the LDOS is strongly localized in the bottom sub-ribbon which is slightly larger than the top one and forms a thin 1D channel.

In summary, we have shown that by introducing a periodic distribution of vacancies in the lattice the effective width of the GNR is reduced with the subsequent reduction of the phonon thermal conductance and the enhancement of the electronic band gap, the Seebeck coefficient and the *ZT* peaks. This theoretical investigation may seem very speculative. However, some recent experimental works [56–59] have suggested the possibility to generate nano-holes in 2D graphene to form a nanomesh lattice. Such nano-holes of several missing atoms (or vacancy groups) have similar effects as single atomic vacancies on the electronic transport. In 2D nanomeshes, the electrons are confined in the sub-ribbons formed between two hole lines and the transport becomes similar to that in 1D GNRs. By adjusting the period and the radius of vacancy groups the effective transport width, the bandgap [60] and thus the electron and hole transport can be modulated. This is confirmed by recent works showing that a bandgap is opened in quasi-metallic GNRs by the introduction of periodical atomic vacancies [61] which may be seen as the limit case of a nanomesh lattices.

3.3 Multi-junction GNRs

The enhancement of thermoelectric properties of GNRs by introducing a periodical distribution of vacancies is too small for designing efficient thermoelectric devices. Here we examine the effect of another type of nanostructuring which consists in a kind of superlattice formed by alternate AGNR sections of different widths. This configuration is referred to as Multi-Junction GNR (MJ-GNR). It has been previously shown that MJ-GNRs with alternate sections of 8-AGNRs and 20-ZGNRs may lead to *ZT* of about 1 [22]. In this Section, we examine first the case of an MJ-GNR made of AGNR sections only, i.e. 8-AGNRs and 16-AGNRs, and then we analyze the combination of this superlattice with the periodic distribution of vacancies.

The simulated MJ-GNR is schematized in Fig. 6(a). The phonon thermal conductance K_{ph} of this structure is compared to that of perfect 8-AGNR and 16-AGNR in Fig. 6(b). As expected from the presence of narrow sections which limit the phonon flux, the thermal conductance is smaller in the MJ-GNR than in the perfect 16-AGNR. It is more surprising to see that it is even smaller than in the perfect 8-AGNR. At room temperature K_{ph} decays from 2.4 nW/K in 16-AGNR to 1.2 nW/K in 8-AGNR and 0.6 nW/K in MJ-AGNR. This over-reduction is a consequence of the mismatch of phonon modes between the AGNR sections of different width which weakens their transmission. In terms of

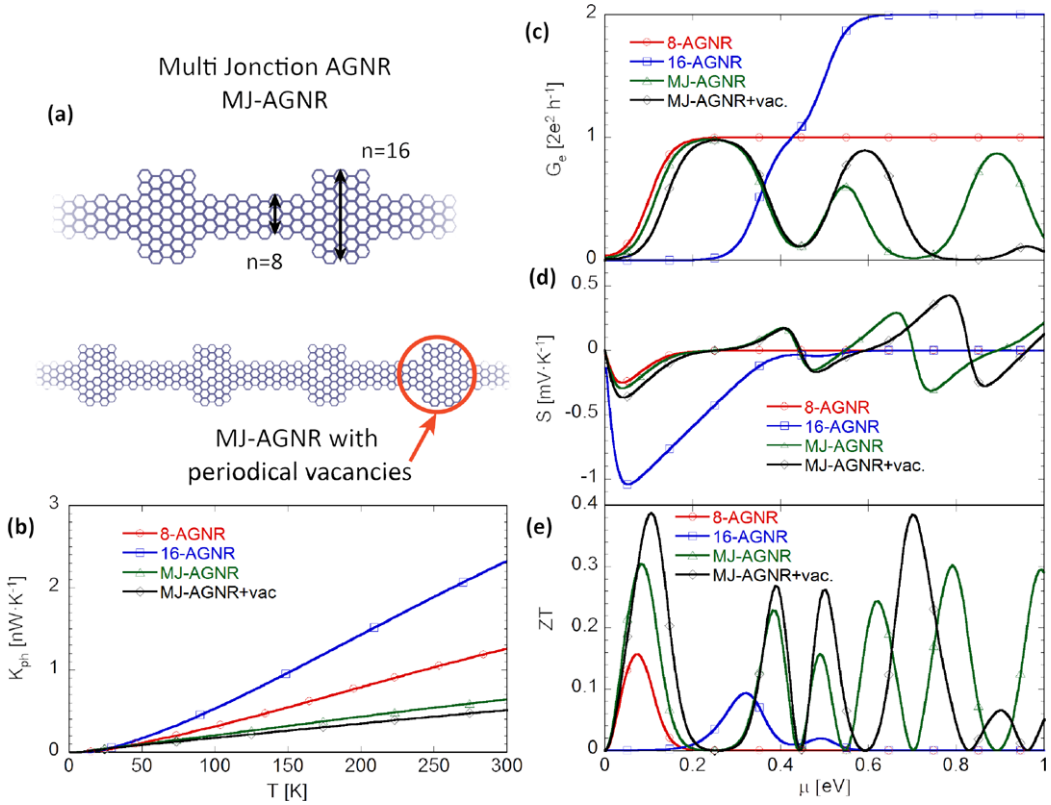

Fig. 6 (**a**) MJ-AGNR structure alternating 8-AGNR and 16-AGNR sections and the same structure with a periodical distribution of atomic vacancies. (**b**) Thermal conductance as a function of temperature T, (**c**) electronic conductance, (**d**) Seebeck coefficient and (**e**) figure of merit ZT as a function of chemical potential μ

thermoelectric properties it may be a clear advantage of this structuring if it is not compensated by a concomitant degradation of the electronic transport properties.

The electronic conductance G_e is plotted for the three structures in Fig. 6(c) and a specific behavior is observed for MJ-GNR. At low chemical potential, the conductance of MJ-GNR is similar to that of 8-AGNR. In this energy range 0 eV–0.3 eV, the conductance of 16-AGNR is nearly zero because of its wide electronic bandgap but the electronic transport in MJ-AGNR seems not to be influenced by the presence of these high-bandgap sections. At higher chemical potential, i.e. beyond the 16-AGNR bandgap, an unexpected phenomenon appears: the coupling between 8-AGNR and 16-AGNR electronic states reduces the conductance which tends to zero, as in the well-known case of resonant tunneling leading to a negative differential conductance (NDC). Strong conductance oscillations are even observed when further increasing the energy. This phenomenon is well illustrated by the electronic transmission function and band structure plotted in Figs. 7(a) and (b), respectively. The formation of energy minigaps and minibands yields the alternation of zero and unity transmission regions and is responsible for the NDC behavior and for the conductance oscillations.

The NDC phenomenon has repercussions on the Seebeck coefficient S shown in Fig. 6(d). In MJ-AGNR, S presents strong oscillations from positive to negative values, which is typical of multi-barrier systems [62]. The analysis of the electronic LDOS as plotted in Figs. 7(c) and (d) supports this interpretation: depending on the energy, some regions of the GNR play the role of barriers while other regions act as dots with quasi-localized states. In Fig. 7(c) we plot the LDOS averaged over the width of the ribbon as a function of the electron energy and the length of the MJ-AGNR. In the miniband energy ranges we can identify periodical zones of high and low DOS. An example of the localization of states is more accurately displayed in Fig. 7(d) where we plot the atomic LDOS calculated at 0.25 eV, i.e. at the position of the first electronic conductance peak. In particular, at this energy the presence of zigzag edges on the sides of the 16-AGNR sections generates localized states of high density, as recently evidenced experimentally [63]. In the minibands, the conduction regime is governed by the resonant transport between such localized states.

The strong oscillations of electron conductance and Seebeck coefficient increase the power factor $G_e S^2$ for several values of chemical potential. Combined with the strong reduction of thermal conductance K_{ph}, this enhancement of

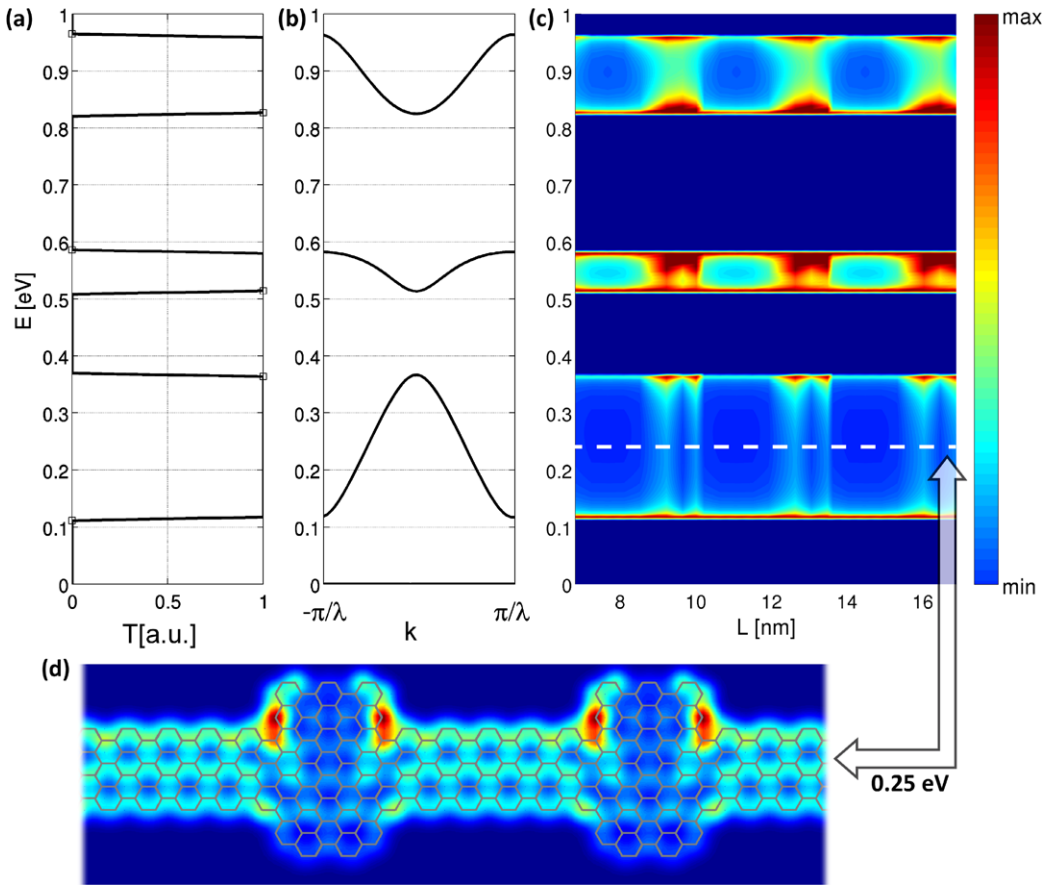

Fig. 7 (**a**) Electronic transmission of MJ-AGNR as a function of electron energy. (**b**) Electronic energy bands as a function the wave vector k. (**c**) Corresponding width-averaged LDOS map in the energy-length space and (**d**) atomic LDOS calculated at 0.25 eV

$G_e S^2$ causes the appearance of several high ZT peaks in MJ-GNR. In Fig. 6(e) we can identify at least four ZT peaks in the energy range 0–0.8 eV with maximum values about twice as high as in AGNRs. For instance the first peak increases from 0.15 for 8-AGNR to 0.3 for MJ-GNR at room temperature. These results are consistent with the recent work reported in [39].

The overall enhancement of thermoelectric properties in MJ-GNR can be further increased by combining this multi-junction structuring with the periodic distribution of vacancies. We have simulated the MJ-GNR device including vacancies in the center of each 16-AGNR section, as schematized in Fig. 6(a). Here the vacancies have the same effect as in perfect AGNRs, i.e. essentially related to the enhancement of bandgap due to the reduction of the effective ribbon width. The results obtained are plotted in all graphs of Fig. 6 (black lines with diamonds). Compared to MJ-GNR without vacancy we observe a small decrease of thermal conductance, a small increase of height and width of S peaks, and a significant increase of ZT which almost reaches the value of 0.4 at room temperature.

4 Conclusion

The Green's function technique has been shown to be a powerful method to describe on the same footing electron and phonon transport in nanodevices on the basis of atomistic material descriptions. It is thus a good approach to studying the thermoelectric device performance at the nanometer scale. It has been applied here to the case of graphene nanoribbons in the ballistic approximation.

Though the reduction of phonon thermal conductance induced by edge disorder or by random vacancies was expected to enhance the thermoelectric figure of merit ZT, this advantage is fully compensated by the concomitant reduction of electronic conductance, which even results in a reduction of ZT compared to perfect AGNRs. However, a periodic distribution of vacancies inside the ribbon may be seen as a reduction of the effective width, which tends to reduce the thermal conductance while enhancing the thermopower. It results in an increase of ZT.

Finally, a specific structuring of GNR obtained by alternating armchair sections of different width has been shown to provide high thermoelectric performance with a ZT factor

reaching 0.3 at room temperature and even 0.4 if periodic vacancies are added in the wide GNR sections. It results from the combination of (i) very small phonon thermal conductance due to the mismatch of phonon modes in the different sections and (ii) the resonant tunneling of electrons between these sections which retains high electron conductance and Seebeck coefficient.

With the expected improvements in the patterning of GNRs at the atomic scale, these results allow us to propose strategies for designing efficient graphene-based thermoelectric nanodevices.

Acknowledgements The authors would like to thank Yann Apertet, Arnaud Bournel, and Damien Querlioz for many useful discussions. This work was partially supported by the French ANR through project NANOSIM_GRAPHENE (ANR-09-NANO-016).

References

1. Bolotin, K.I., Sikes, K.J., Jiang, Z.d., Klima, M., Fudenberg, G., Hone, J., Kim, P., Stormer, H.L.: Ultrahigh electron mobility in suspended graphene. Solid State Commun. **146**, 351–355 (2008)
2. Schwierz, F.: Graphene transistors. Nat. Nanotechnol. **5**, 487–496 (2010)
3. Balandin, A.A., Ghosh, S., Bao, W., Calizo, I., Teweldebrhan, D., Miao, F., Lau, C.N.: Superior thermal conductivity of single-layer graphene. Nano Lett. **8**, 902–907 (2008)
4. Ghosh, S., Calizo, I., Teweldebrhan, D., Pokatilov, E.P., Nika, D.L., Balandin, A.A., Bao, W., Miao, F., Lau, C.N.: Extremely high thermal conductivity of graphene: Prospects for thermal management applications in nanoelectronic circuits. Appl. Phys. Lett. **92**, 151911 (2008)
5. Cai, W., Moore, A.L., Zhu, Y., Li, X., Chen, S., Shi, L., Ruoff, R.S.: Thermal transport in suspended and supported monolayer graphene grown by chemical vapor deposition. Nano Lett. **10**, 1645–1651 (2010)
6. Zuev, Y.M., Chang, W., Kim, P.: Thermoelectric and magnetothermoelectric transport measurements of graphene. Phys. Rev. Lett. **102**, 096807 (2009)
7. Wei, P., Bao, W., Pu, Y., Lau, C.N., Shi, J.: Anomalous thermoelectric transport of Dirac particles in graphene. Phys. Rev. Lett. **102**, 166808 (2009)
8. Goldsmid, H.J., Douglas, R.W.: The use of semiconductors in thermoelectric refrigeration. Br. J. Appl. Phys. **5**, 386–390 (1954)
9. Hicks, L.D., Dresselhaus, M.S.: Effect of quantum-well structures on the thermoelectric figure of merit. Phys. Rev. B **47**, 12727–12731 (1993)
10. Hicks, L.D., Harman, T.C., Sun, X., Dresselhaus, M.S.: Experimental study of the effect of quantum-well structures on the thermoelectric figure of merit. Phys. Rev. B **53**, R10493–R10496 (1996)
11. Venkatasubramanian, R., Siivola, E., Colpitts, T., O'Quinn, B.: Thin-film thermoelectric devices with high room-temperature figures of merit. Nature **413**, 597–602 (2001)
12. Zide, J.M.O., Vashaee, D., Bian, Z.X., Zeng, G., Bowers, J.E., Shakouri, A., Gossard, A.C.: Demonstration of electron filtering to increase the Seebeck coefficient in $In_{0.53}Ga_{0.47}As/In_{0.53}Ga_{0.28}Al_{0.19}As$ superlattices. Phys. Rev. B **74**, 205335 (2006)
13. Harman, T.C., Taylor, P.J., Walsh, M.P., LaForge, B.E.: Quantum dot superlattice thermoelectric materials and devices. Science **297**, 2229–2232 (2002)
14. Tsaousidou, M., Triberis, G.P.: Thermoelectric properties of a weakly coupled quantum dot: Enhanced thermoelectric efficiency. J. Phys., Condens. Matter **22**, 355304 (2010)
15. Shi, L., Yao, D., Zhang, G., Li, B.: Large thermoelectric figure of merit in $Si_{1-x}Ge_x$ nanowires. Appl. Phys. Lett. **96**, 173108 (2010)
16. Hochbaum, A.I., Chen, R., Delgado, R.D., Liang, W., Garnett, E.C., Najarian, M., Majumdar, A., Yang, P.: Enhanced thermoelectric performance of rough silicon nanowires. Nature **451**, 163–167 (2008)
17. Boukai, A.I., Bunimovich, Y., Tahir-Kheli, J., Yu, J.-K., Goddard, W.A. III, Heath, J.R.: Silicon nanowires as efficient thermoelectric materials. Nature **451**, 168–171 (2008)
18. Ni, X., Liang, G., Wang, J.-S., Li, B.: Disorder enhances thermoelectric figure of merit in armchair graphane nanoribbons. Appl. Phys. Lett. **95**, 192114 (2009)
19. Sevinçli, H., Cuniberti, G.: Enhanced thermoelectric figure of merit in edge-disordered zigzag graphene nanoribbons. Phys. Rev. B **81**, 113401 (2010)
20. Ouyang, T., Chen, Y.P., Yang, K.K., Zhong, J.X.: Thermal transport of isotopic-superlattice graphene nanoribbons with zigzag edge. Europhys. Lett. **88**, 28002 (2009)
21. Karamitaheri, H., Pourfath, M., Faez, R., Kosina, H.: Geometrical effects on the thermoelectric properties of ballistic graphene antidot lattices. J. Appl. Phys. **110**, 054506 (2011)
22. Mazzamuto, F., Hung Nguyen, V., Apertet, Y., Caër, C., Chassat, C., Saint-Martin, J., Dollfus, P.: Enhanced thermoelectric properties in graphene nanoribbons by resonant tunneling of electrons. Phys. Rev. B **83**, 235426 (2011)
23. Lacroix, D., Joulain, K., Terris, D., Lemonnier, D.: Monte Carlo simulation of phonon confinement in silicon nanostructures: Application to the determination of the thermal conductivity of silicon nanowires. Appl. Phys. Lett. **89**, 103104 (2006)
24. Volz, S., Chen, G.: Molecular dynamics simulation of thermal conductivity of silicon nanowires. Appl. Phys. Lett. **75**, 2056–2058 (1999)
25. Hu, J., Ruan, X., Chen, Y.P.: Thermal conductivity and thermal rectification in graphene nanoribbons: A molecular dynamics study. Nano Lett. **9**, 2730–2735 (2009)
26. Shi, L.-P., Xiong, S.-J.: Phonon thermal conductance of disordered graphene strips with armchair edges. Phys. Lett. A **373**, 563–569 (2009)
27. Li, W., Sevinçli, H., Haldun, G., Cuniberti, G., Roche, S.: Phonon transport in large scale carbon-based disordered materials: Implementation of an efficient order-N and real-space Kubo methodology. Phys. Rev. B **82**, 041410 (2010)
28. Lan, J., Wang, J.-S., Gan, C.K., Chin, S.K.: Edge effects on quantum thermal transport in graphene nanoribbons: Tight-binding calculations. Phys. Rev. B **79**, 115401 (2009)
29. Nam Do, V., Hung Nguyen, V., Dollfus, P., Bournel, A.: Electronic transport and spin-polarized effects of relativistic-like particles in graphene structures. J. Appl. Phys. **104**, 063708 (2008)
30. Ouyang, Y., Campbell, P., Guo, J.: Analysis of ballistic monolayer and bilayer graphene field-effect transistors. Appl. Phys. Lett. **92**, 063120 (2008)
31. Hung Nguyen, V., Bournel, A., Lien Nguyen, V., Dollfus, P.: Resonant tunneling and negative transconductance in single barrier bilayer graphene structure. Appl. Phys. Lett. **95**, 232115 (2009)
32. Fiori, G., Iannaccone, G.: Simulation of graphene nanoribbon field-effect transistors. IEEE Electron Device Lett. **28**, 760–762 (2007)
33. Gunlycke, D., Areshkin, D.A., White, C.T.: Semiconducting graphene nanostrips with edge disorder. Appl. Phys. Lett. **90**, 142104 (2007)
34. Liang, G., Neophytou, N., Lundstrom, M.S., Nikonov, D.E.: Ballistic graphene nanoribbon metal-oxide-semiconductor field-

effect transistors: A full real-space quantum transport simulation. J. Appl. Phys. **102**, 054307 (2007)
35. Hung Nguyen, V., Nam Do, V., Bournel, A., Lien Nguyen, V., Dollfus, P.: Controllable spin-dependent transport in armchair graphene nanoribbon structures. J. Appl. Phys. **106**, 053710 (2009)
36. Zhao, P., Chauhan, J., Guo, J.: Computational study of tunnelling transistor based on graphene nanoribbon. Nano Lett. **9**, 684–688 (2009)
37. Nam Do, V., Dollfus, P.: Negative differential resistance in zigzag-edge graphene nanoribbon junctions. J. Appl. Phys. **107**, 063705 (2010)
38. Hung Nguyen, V., Mazzamuto, F., Saint-Martin, J., Bournel, A., Dollfus, P.: Giant effect of negative differential conductance in graphene nanoribbon p-n heterojunctions. Appl. Phys. Lett. **99**, 042105 (2011)
39. Chen, Y., Jayasekera, T., Calzolari, A., Kim, K.W., Nardelli, M.B.: Thermoelectric properties of graphene nanoribbons, junctions and superlattices. J. Phys., Condens. Matter **22**, 372202 (2010)
40. Mohr, M., Maultzsch, J., Dobardzic, E., Reich, S., Milosevic, I., Damnjanovic, M., Bosak, A., Krisch, M., Thomsen, C.: Phonon dispersion of graphite by inelastic x-ray scattering. Phys. Rev. B **76**, 035439 (2007)
41. Mazzamuto, F., Saint-Martin, J., Valentin, A., Chassat, C., Dollfus, P.: Edge shape effect on vibrational modes in graphene nanoribbons: A numerical study. J. Appl. Phys. **109**, 064516 (2011)
42. Neophytou, N., Kosina, H.: Thermoelectric properties of scaled silicon nanowires using the $sp^3d^5s^*$-SO atomistic tight-binding model and Boltzmann transport. J. Electron. Mater. **40**, 753–758 (2011)
43. Novoselov, K.S., Geim, A.K., Morozov, S.V., Jiang, D., Zhang, Y., Dubonos, S.V., Grigorieva, I.V., Firsov, A.A.: Electric field effect in atomically thin carbon films. Science **306**, 666–669 (2004)
44. Betti, A., Fiori, G., Iannaccone, G.: Atomistic investigation of low-field mobility in graphene nanoribbons. IEEE Trans. Electron Devices **58**, 2824–2830 (2011)
45. Gunlycke, D., Lawler, H.M., White, C.T.: Room-temperature ballistic transport in narrow graphene strips. Phys. Rev. B **75**, 085418 (2007)
46. Reich, S., Maultzsch, J., Thomsen, C., Ordejón, P.: Tight-binding description of graphene. Phys. Rev. B **66**, 035412 (2002)
47. Son, Y.-W., Cohen, M.L., Louie, S.G.: Energy gaps in graphene nanoribbons. Phys. Rev. Lett. **97**, 216803 (2006); (Err) Phys. Rev. Lett. **98**, 089901 (2007)
48. Lu, Q., Huang, R.: Excess energy and deformation along free edges of graphene Nanoribbons. Phys. Rev. B **81**, 155410 (2010)
49. Datta, S.: Nanoscale device modeling: The Green's function method. Superlattices Microstruct. **28**, 253–278 (2000)
50. Sancho, M.P.L., Sancho, J.M.L., Rubio, J.: Quick iterative scheme for the calculation of transfer matrices: Application to Mo (100). J. Phys. F, Met. Phys. **14**, 1205–1215 (1984)
51. Anantram, M., Lundstrom, M., Nikonov, D.: Modeling of nanoscale devices. Proc. IEEE **96**, 1511–1550 (2008)
52. Sivan, U., Imry, Y.: Multichannel Landauer formula for thermoelectric transport with application to thermopower near the mobility edge. Phys. Rev. B **33**, 551–558 (1986)
53. Mingo, N.: Calculation of Si nanowire thermal conductivity using complete phonon dispersion relations. Phys. Rev. B **68**, 113308 (2003)
54. Mazzamuto, F.: Etude théorique des propriétés thermiques et thermoélectriques des nanorubans de graphene. PhD dissertation, Univ. Paris-Sud, Orsay (2011) (in French)
55. Goldsmid, H.J., Sharp, J.W.: Estimation of the thermal band gap of a semiconductor from Seebeck measurements. J. Electron. Mater. **28**, 869–872 (1999)
56. Bai, J., Zhong, X., Jiang, S., Huang, Y., Duan, X.: Graphene nanomesh. Nat. Nanotechnol. **5**, 190–194 (2010)
57. Akhavan, O.: Graphene nanomesh by ZnO nanorod photocatalysts. ACS Nano **4**, 4174–4180 (2010)
58. Kim, M., Safron, N.S., Han, E., Arnold, M.S., Gopalan, P.: Fabrication and characterization of large-area, semiconducting nanoperforated graphene materials. Nano Lett. **10**, 1125–1131 (2010)
59. Liang, X., Jung, Y.-S., Wu, S., Ismach, A., Olynick, D.L., Cabrini, S., Bokor, J.: Formation of bandgap and subbands in graphene nanomeshes with sub-10 nm ribbon width fabricated via nanoimprint lithography. Nano Lett. **10**, 2454–2460 (2010)
60. Petersen, R., Pedersen, T.G.: Quasiparticle properties of graphene antidot lattices. Phys. Rev. B **80**, 113404b (2009)
61. Martinazzo, R., Casolo, S., Tantardini, G.F.: Symmetry-induced band-gap opening in graphene superlattices. Phys. Rev. B **81**, 245420 (2010)
62. Larsson, M., Antonyuk, V.B., Mal'shukov, A.G., Chao, K.A.: Thermopower anomaly in multiple barrier structures. Phys. Rev. B **68**, 233302 (2003)
63. Ritter, K.A., Lyding, J.W.: The influence of edge structure on the electronic properties of graphene quantum dots and nanoribbons. Nat. Mater. **8**, 235–242 (2009)